Nonstatistical effects observed with ^{52}Cr+n resonances

G. Rohr, R. Shelley, and A. Brusegan

Commission of the European Communities, Joint Research Centre, Central Bureau for Nuclear Measurements, Geel, Belgium

F. Poortmans and L. Mewissen

Studiecentrum voor Kernenergie, Mol, Belgium

(Received 31 May 1988)

The neutron total and neutron capture cross sections of ^{52}Cr have been measured using the neutron time-of-flight technique at a pulsed electron linear accelerator. Data analyses have been performed in the energy ranges 1 to 500 keV and 1 keV to 1 MeV, respectively, for capture and transmission, with R-matrix multilevel multichannel codes and with resonance shape fitting procedures, to determine the resonance parameters E_0, $g\Gamma_n$, $g\Gamma_\gamma$, J, and l. Subsequent values for the average resonance parameters for s-wave and p-wave neutron resonances are $D_0 = (43.4 \pm 4.7)$ keV and $S_0 = (2.85 \pm 0.25) \times 10^{-4}$ up to 1 MeV, and $D_1 = 14.7$ keV and $S_1 = (0.30 \pm 0.05) \times 10^{-4}$ up to 200 keV. The following nonstatistical effects are indicated in the resonance parameter set: two gaps are observed in the s-wave level distribution, where at least two resonances for each gap are missing; a strong discontinuity in the level spacing is observed for p-wave resonances whereby three energy ranges, up to 500 keV, with different level spacings may be distinguished. This energy-dependent behavior of the p-wave level density shows that the level density parameter (a) strongly depends on the excitation energy and causes parity dependence of nuclear states in the neutron energy range (200–500) keV. These deviations of the resonance parameters from statistical behavior may be explained by doorway structures with a small energy spread of states, as has been observed for ^{28}Si and ^{32}S which, like ^{52}Cr, have a multiple of four nucleons in the target nucleus.

I. INTRODUCTION

The cross section of ^{52}Cr is important for reactor applications because this nuclide, after ^{56}Fe, is the next major component of stainless steel which is used as a structural material. The resonance data are also of significant physical interest because this nucleus has a relatively small number of protons (24) and neutrons (28) with a closed neutron shell. Therefore the level density of states at neutron separation energy is small (30 states per MeV) and according to the level density systematics[1] the number of particles (p) and holes (h), i.e., quasiparticles, participating in the excitation process is either 2p-1h or maximum 3p-2h.

The consequences of these excitation characteristics are as follows: the resonance parameters may have nonstatistical properties because the compound state is created by one, or maximum two, collisions of nucleons in the nucleus. Correlation between the total radiative width (Γ_γ) and the reduced neutron width would indicate this effect and has been studied elsewhere.[2] The large spacing of single-particle states near the Fermi surface energy and the small number of particles and holes participating in the excitation lead to the fact that only a few single-particle states contribute to the excitation. Whether or not, in this case, the excited states are equally distributed with respect to the parity of states depends on the (local) single-particle spectrum. Furthermore, the strength function values can deviate from the optical model due to

changes in the doorway level density at neutron separation energy.[3] This effect should be large for $A = 53$ because of the low hierarchy of the compound states and the fact that ^{52}Cr is in the peak of the s-wave strength function.

The excitation properties can also cause problems when measuring the neutron capture cross section. A low multiplicity (1 or 2) of the gamma rays produced in the deexcitation process leads to a very hard gamma-ray spectrum with changes in the hardness from one resonance to another. The application of the weighting technique on such hard spectra can result in a variation, compared with the measured yield, which strongly depends upon the weighting function itself.

Recently, resonance data for ^{53}Cr and ^{55}Cr have been published up to an energy of 900 keV.[4] In both nuclei parity dependences for s- and p-wave resonances have been observed. Partial results up to 500 keV of the present work have been published at the International Nuclear Data Conference in Santa Fe.[5] The goal of the present measurements is to substantially improve the resolution of the total cross-section measurements and, in addition, to include capture measurements to enhance the data set, especially for narrow resonances. This will allow us to study the above mentioned nonstatistical effects more thoroughly.

II. EXPERIMENT

The measurements were performed at the 150 MeV Geel linac (GELINA), operating with a burst width of

4.5 ns and a frequency of 800 Hz, using five neutron flight paths with lengths ranging from 28 to 400 m. The samples used were chromium-oxide (Cr_2O_3) powder enriched to a purity of 99.74% and obtained on loan from the Oak Ridge National Laboratory (ORNL) Isotope Division. The powder was canned in thin aluminum containers of 8 cm diameter (for the capture and 50 m transmission measurements) or 3.5 cm diameter (for the 200 and 400 m transmission measurements) with 0.0114 and 0.0593 chromium atoms/b, respectively.

A. Transmission measurements

Total neutron cross-section measurements were performed at the 50, 200, and 400 m flight-path stations with the neutron beam emerging from the uranium target of the linac being moderated for the two shorter-distance experiments but not for that at 400 m. The time-of-flight detection system for the 50 m measurement consisted of a $^{10}B_4C$ slab (5 mm thick) viewed by two 10.2×7.6 cm NaI(Tl) detectors, situated out of the neutron beam, registering neutron transmission events via the 478 keV gamma ray associated with neutron absorption in the ^{10}B. The resulting pulses were processed by a "fast-slow" electronic system linked to a 10 ns Technical Measurement Corp. (TMC) time coder and stored in a 4 ns channel TMC analyzer (1.4 μs total dead time). A BF_3 detector was used as reference in the cyclic sample-in and sample-out (of the beam) measurements. A $^{10}B_4C$ slab (0.4 g/cm^2) was placed in the beam as an antioverlap filter to absorb low-energy neutrons and the background was determined from the black resonance minima using Bi, Na, and S filters.

In the 200 and 400 m measurements a 25 mm thick Nuclear Enterprises NE110 plastic scintillator was viewed by four RCA 4516 photomultipliers and, in addition to the antioverlap filters, a significant reduction of the gamma flash effect in this detector was obtained by filtering the beam with 0.37 g/cm^2 of uranium. The time-of-flight events analyzer consisted of a 4 ns time digitizer interfaced via a double data buffer (2×128 words, each 32 bits) to a Hewlett-Packard 2113E computer with 96 000 words of memory available for data storage. A count rate in excess of 10^4 events/sec could be handled and the dead time after each event was only 540 ns. (The maximum value for the dead-time correction was 10% without the sample in the beam.) In order to optimize the signal-to-background ratio the pulse-height range was divided into four windows and only those time-of-flight events for which the pulse height was within the required window were stored. Background was due to almost constant activities in the detector room and long-lived radiations from the neutron source and was measurable at long flight times immediately before the arrival of the next neutron burst. In the 200 m moderated neutron-beam experiment an additional background arising from the 2.2 MeV gamma rays produced by neutron capture in the moderator itself had to be taken into account as the plastic scintillator was in the neutron beam.

The neutron energy resolution width ΔE (FWHM) is obtained from the following expression:

$$(\Delta E/E)^2 = (2\Delta L/L)^2 + (2\Delta t/t)^2$$

$$= (0.020 + 0.18E) \times 10^{-6}$$

In this expression L is the flight-path length in m, t is the total flight time of neutrons with energy E (MeV), and ΔL and Δt are the corresponding uncertainties. Typical values of ΔE (FWHM) at 400 m are 64 eV at 250 keV, 166 eV at 550 keV, and 450 eV at 1 MeV. The influence of the moderator, when used, on the resolution function has been included using the results of the Monte Carlo simulation from Ref. 6. The resolution function has been carefully checked by shape fitting very narrow resonances.

B. Capture measurements

The main neutron capture was conducted at the 60 m flight-path station of the linac with a moderated neutron beam collimated by means of copper and lead cylinders to give a 6.5 cm beam diameter at the sample. The sample was viewed edgewise by cylindrical C_6D_6 liquid scintillators of 10.2 cm diameter and 7.6 cm height placed with their axes perpendicular to the neutron beam and 180° apart. The detectors were unshielded and the surrounding material minimized in order to reduce the prompt background originating from neutron scattering. Each detected neutron-capture gamma-ray event was analyzed in time by a 4 ns multi-stop time coder and amplitude sorted by an analogue-to-digital converter with 256 channels, the total dead time being 3.6 μs. The linearity of the detector system was checked with the Compton edge energy of various gamma-ray sources and the gain stability regularly controlled with the 6.13 MeV peak of a ^{238}Pu-$^{13}C(\alpha, n_\gamma)^{16}O$ source.

Only those capture events detected producing electron energies above 150 keV were accepted by a multiparameter acquisition system which sorted and stored data into 256 pulse-height and 16 000 time-of-flight channels. Each count was weighted according to its amplitude so as to produce a detector efficiency proportional to the total gamma-ray energy released by capture events. The weighting technique is described in detail in Ref. 7 and the weighting function used is discussed in Ref. 8. Neutron flux measurements were performed under identical experimental conditions as those of the capture yield by simply replacing the ^{52}Cr sample with a 3 mm thick $^{10}B_4C$ slab and detecting the 478 keV photons associated with the $^{10}B(n, \alpha_\gamma)^7Li$ reaction. Additionally, an independent flux determination was made using 0.5 mm thick ^6Li glass. For each flux measurement a background measurement was made by determining the count rates at the minima of "black"' resonances present in the neutron spectrum transmitted through Ag, Bi, Co, Na, S, and W filters. The neutron flux curves obtained from the B and Li data were corrected for background, the detection efficiency, self-screening and multiple scattering effects and found to agree within 3% in the energy range 1–300 keV where comparison was made. The neutron sensitivity of the C_6D_6 capture detectors was measured independently.[9]

For reasons that will be explained in the next section a

completely separate neutron capture experiment was undertaken to confirm the 50 m transmission result for the resonance at 1.63 keV. Using a natural chromium sample containing 8.592×10^{21} atoms/cm^2 at a flight path of 28 m, the events registered by the two C_6D_6 detectors were weighted, as before, but then stored on a Nuclear Data ND 6600 acquisition system. The sample was then replaced by a 1 mm Ag sample and the measurement repeated enabling us to use five Ag resonances, in the energy range 16–71 eV, for normalization. The neutron flux, using the 0.5 mm thick Li glass, and the background were measured as explained above.

III. NORMALIZATION (OF THE CAPTURE DATA)

As reported in an earlier paper[8] a discrepancy exists for the 1.15 keV resonance in ^{56}Fe, between the neutron resonance parameters deduced from transmission and those from capture measurements. This discrepancy has led to the ^{56}Fe task force[10] and is still not satisfactorily explained. Therefore prior to analyzing the capture data from our 60 m measurement of ^{52}Cr we conducted the special capture normalization run at 28 m to obtain better statistics for the 1.63 keV resonance. This is an almost pure neutron capture resonance ($\Gamma_\gamma \ll \Gamma_n$) and the parameters deduced for it, normalized to five well-known Ag resonances, have been compared to the 50 m transmission result. Both results for this resonance are given in Table I. The fact that the capture area (A), used to normalize the main capture data, and the transmission result are within the given errors indicates that the gamma-ray spectrum of the 1.63 keV resonance is weak.

Furthermore, the (relative) hardness of this gamma-ray spectrum has been determined by taking the ratio w of the resonance areas calculated from the weighted and unweighted spectra. For this resonance $w = 13$, compared with $w = 11$ for the Ag resonances which are known to have weak gamma-ray spectra. The 1.15 keV resonance of ^{58}Fe, known to have a strong gamma-ray spectrum, has a ratio $w = 29$ and this led to the discrepancy of approximately 20% between its neutron capture and transmission results. However, the 1.6 keV resonance of ^{57}Fe, with $w = 21$, had no such discrepancy.[8] The ratio for the seven lowest energy ^{52}Cr levels is in the range $w = 15.5 \pm 3.5$ and we can therefore confidently determine the capture areas of resonances in this isotope.

IV. DATA ANALYSIS

A. Transmission

The neutron transmission spectra of the 50 m experiment have been analyzed by two independent shape-fitting computer programs in the energy range up to 100 keV. Firstly with SIOB,[11] a multilevel Breit-Wigner fitting routine in which the calculation of the total cross section closely follows the formulation of Bhat[12] and Gregson et al.[13] Although the analysis yields the product $g\Gamma_n$ for each resonance, where the statistical weight factor $g = (2J+1)/2(2I+1)$, J is the resonance spin, and $I = 0$ is the ground-state spin of the ^{52}Cr nucleus, the use of this program has been limited to well-isolated non-s-wave resonances with no interference effects, such as that at

1.63 keV. The second program used was FANAL,[14] which incorporates an R-matrix formalism for the s-wave resonances and correctly takes into account strong interferences. A Breit-Wigner formula for non-s-wave resonances and Doppler broadening is included and the description is acceptable at the lower energies of this run, as p-wave resonances are well separated and have small neutron widths so that level-level interference is negligible. In the literature several Debye temperatures are given for natural chromium, ranging from 405 to 685 K. From our experience with zirconium,[15] oxide samples have a higher Debye temperature than natural ones and we have therefore taken the value 606 K from Ref. 16 which is higher than the average literature value for natural chromium. This results in an effective temperature of 353 K for chromium-oxide.

The two other transmission measurements have been analyzed in the energy range 90–900 keV by the Reich-Moore multilevel program MULTI (Ref. 17) with a nuclear radius $R' = (5.5 \pm 0.5)$ fm. Neutron widths were determined from the shape analysis; spin and parity were assigned as follows: (1) s-wave resonances were easily detected because of the strong resonance-potential interference effect; (2) assignment of $l = 1$ or $l = 2$ could be done on the basis of the resonance shape whereby $l = 1$ resonances show asymmetric shape due to interference with p-wave scattering, whereas $l = 2$ resonances do not; (3) spin assignment was based upon the peak total cross section; (4) in certain cases l and J assignment was possible on the basis of observed resonance-resonance interference. The experimental spectra were corrected for background, dead time and the influence of the oxygen cross section and then reduced to pure chromium transmission spectra using ANGELA,[18] a system program used at the Central Bureau for Nuclear Measurements (CBNM) for the off-line reduction of nuclear data.

B. Capture

For the neutron capture experiments the background contribution in the capture yield has been determined at minima in the spectra between well-separated resonances and described with a monotonic function over the complete energy range of interest. After subtraction of this background, correction for the neutron flux and normalization, the weighted counting rates can be reduced to the neutron capture cross-section spectra. These are still Doppler and resolution broadened and are not corrected for multiple scattering nor prompt background contributions. Analysis has therefore been performed with the capture area fitting program based upon TACASI,[19] which utilizes a single-level Breit-Wigner formalism, and with the R-matrix resonance shape-fitting program FANAC.[20] The latter is necessary for analyzing large s-wave resonances in order to account for the complicated self-screening and multiple scattering effects. Wherever possible results from our transmission experiments have been used as fixed parameters in the capture analysis. Prompt background due to the detection of events caused by capture of scattered neutrons in the surroundings, so-called neutron sensitivity of the capture detectors, has been taken into account when analyzing large s-wave resonances.

TABLE I. Parameters E_0, J, l, $g\Gamma_n$, $g\Gamma_Y$, and A $(=g\Gamma_n\Gamma_Y/\Gamma)$ of 200 resonances in ^{52}Cr.

E_0 (keV)	J l	$g\Gamma_n$ (eV)	$\Delta g\Gamma_n$	$g\Gamma_Y$ (eV)	$\Delta g\Gamma_Y$	A (eV) ΔA
1.627±0.001	$(\frac{3}{2}$ 1)	0.0624±	0.002	1.34 ±	0.28	0.058±0.003
19.40 ±0.01						0.017±0.003
22.98 ±0.01	$(\frac{3}{2}$ 1)	7.0 ±	1.0	0.57 ±	0.01	0.53 ±0.02
27.63 ±0.02						0.58 ±0.02
31.68 ±0.02	$\frac{1}{2}$ 0	18.5 ±	1.5	0.24 ±	0.02	0.24 ±0.02
33.96 ±0.02						0.28 ±0.01
34.36 ±0.02						0.18 ±0.01
46.39 ±0.04						0.03 ±0.01
48.00 ±0.02						0.31 ±0.01
48.31 ±0.02	1	11.0 ±	2.0	0.41 ±	0.02	0.40 ±0.02
50.12 ±0.03						0.15 ±0.02
50.30 ±0.06	$\frac{1}{2}$ 0	1620 ±	60	0.49 ±	0.09	0.49 ±0.09
57.78 ±0.05	$(\frac{1}{2}$ 1)	87 ±	6	0.67 ±	.05	0.67 ±0.10[a]
68.23 ±0.03						0.12 ±0.01
78.89 ±0.04						0.38 ±0.02
94.97 ±0.03	$\frac{3}{2}$ 1	100 ±	10			0.54 ±0.03
96.83 ±0.07	$\frac{1}{2}$ 0	8000 ±	900	5.2 ±	2	5.2 ±2.00
106.45 ±0.02		25 ±	3	1.29 ±	0.05	1.23 ±0.05
109.82 ±0.05						0.98 ±0.08
111.80 ±0.02		10 ±	3	1.44 ±	0.40	1.26 ±0.06
113.04 ±0.07						0.50 ±0.04
115.09 ±0.07						0.39 ±0.03
121.92 ±0.05	$\frac{1}{2}$ 0	750 ±	100	1.00 ±	0.15	1.00 ±0.15
122.91 ±0.03		8 ±	4	1.77 ±	0.60	1.45 ±0.07
130.65 ±0.03	$\frac{3}{2}$ 1	250 ±	20	1.82 ±	0.04	1.81 ±0.08
139.49 ±0.03	$\frac{1}{2}$ 1	175 ±	10	1.40 ±	0.07	1.39 ±0.07
140.20 ±0.08	$\frac{1}{2}$ 0	7000 ±	900	0.8 ±	0.3	0.8 ±0.30
143.51 ±0.10						0.38 ±0.05
152.98 ±0.10						1.36 ±0.11
164.94 ±0.10						0.97 ±0.10
166.11 ±0.10						0.33 ±0.07
177.03 ±0.04		25 ±	5	0.71 ±	0.07	0.69 ±0.06
184.97 ±0.04	$\frac{1}{2}$ 1	130 ±	10	1.00 ±	0.07	0.99 ±0.07
0190.27 ±0.04		65 ±	6.0	2.77 ±	0.15	2.66 ±0.15
198.55 ±0.05		65 ±	6.0	0.98 ±	0.08	0.97 ±0.08
199.55 ±0.25						0.13 ±0.07
201.44 ±0.05		40 ±	5.0	1.97 ±	0.15	1.88 ±0.13
204.92 ±0.15						0.86 ±0.10
206.94 ±0.18						1.15 ±0.10
225.07 ±0.20						0.91 ±0.10
231.64 ±0.06	$\frac{3}{2}$ 1	150 ±	12	0.91 ±	0.05	0.90 ±0.09
235.00 ±0.06	$\frac{3}{2}$ 1	180 ±	17	4.82 ±	0.15	4.69 ±0.30
236.95 ±0.12	$\frac{1}{2}$ 1	1100 ±	30	0.79 ±	0.21	0.79 ±0.21
243.23 ±0.03	1	84 ±	7	1.46 ±	0.12	1.44 ±0.12
245.40 ±0.23						0.40 ±0.07
247.40 ±0.07	$\frac{3}{2}$ 1	896 ±	44	0.88 ±	0.12	0.88 ±0.23
249.07 ±0.24						0.16 ±0.08
250.53 ±0.07	$\frac{1}{2}$ 1	461 ±	30	1.56 ±	0.50	1.55 ±0.50

TABLE I. (*Continued*).

E_0 (keV)	J l	$g\Gamma_n$ (eV)	$\Delta g\Gamma_n$	$g\Gamma_Y$ (eV)	$\Delta g\Gamma_Y$	A (eV) ΔA
251.65 ±0.07	$\frac{1}{2}$ 1	362	± 25	0.91 ±	0.35	0.91 ±0.35
258.20 ±0.04	$\frac{3}{2}$ 1	614	± 30	0.88 ±	0.08	0.88 ±0.15
260.93 ±0.25						0.17 ±0.05
265.13 ±0.08	$\frac{1}{2}$ 0	248	± 30	0.21 ±	0.08	0.21 ±0.08
267.34 ±0.27						0.59 ±0.25
274.09 ±0.27						0.83 ±0.12
283.29 ±0.04	$\frac{1}{2}$ 1	770	± 50	0.71 ±	0.40	0.71 ±0.37
283.73 ±0.06		10	± 3	1.55 ±	0.30	1.35 ±0.26
284.75 ±0.04	($\frac{3}{2}$ 1)	40	± 2.5	0.78 ±	0.24	0.77 ±0.24
289.91 ±0.30						0.57 ±0.12
295.41 ±0.05		51	± 8	0.75 ±	0.15	0.74 ±0.15
305.03 ±0.05	$\frac{5}{2}$ 2	585	± 70	3.80 ±	0.10	3.78 ±0.30
307.31 ±0.05	$\frac{3}{2}$ 1	250	± 35	2.05 ±	0.18	2.03 ±0.18
311.76 ±0.10	$\frac{1}{2}$ 1	720	± 35	1.67 ±	0.18	1.67 ±0.18
317.27 ±0.05		52	± 10	0.87 ±	0.12	0.86 ±0.12
324.20 ±0.35						0.37 ±0.10
325.60 ±0.30	$\frac{1}{2}$ 0	10 000	± 500			0.37 ±0.10
330.07 ±0.05	$\frac{3}{2}$ 1	190	± 13	0.24 ±	0.05	0.24 ±0.10
330.95 ±0.05	$\frac{1}{2}$ 1	110	± 9	2.25 ±	0.21	2.20 ±0.21
338.72 ±0.37						1.39 ±0.16
346.00 ±0.06	$\frac{1}{2}$ 1	171	± 12			5.13 ±0.55[b]
347.01 ±0.06	$\frac{3}{2}$ 1	680	± 40			
352.72 ±0.06	$\frac{1}{2}$ 1	185	± 13	0.77 ±	0.30	0.77 ±0.30
353.43 ±0.06	$\frac{3}{2}$ 1	140	± 11	1.90 ±	0.15	1.87 ±0.30
356.90 ±0.40						0.83 ±0.21
362.65 ±0.06		30	± 15	1.40 ±	0.20	1.34 ±0.20
366.50 ±0.25	$\frac{1}{2}$ 0	6 500	± 400			
378.00 ±0.07		100	± 10			
378.62 ±0.07	$\frac{1}{2}$ 1	580	± 41			2.58 ±0.30
386.41 ±0.07	$\frac{3}{2}$ 1	600	± 43	2.88 ±	0.15	2.87 ±0.30[b]
393.76 ±0.07		88	± 18	1.40 ±	0.23	1.38 ±0.22
399.50 ±0.10	$\frac{1}{2}$ 1	529	± 42			
400.03 ±0.25	$\frac{1}{2}$ 0	30 000	±3000			
403.28 ±0.07	$\frac{3}{2}$ 1	203	± 20	1.51 ±	0.11	1.50 ±0.21
419.75 ±0.08	$\frac{1}{2}$ 1	146	± 15	0.87 ±	0.32	0.86 ±0.32
422.35 ±0.20	$\frac{1}{2}$ 0	3 000	± 300			
422.36 ±0.50						0.54 ±0.28
426.46 ±0.08	($\frac{1}{2}$ 1)	240	± 25	1.64 ±	0.40	1.63 ±0.40
434.40 ±0.50						2.58 ±0.64
446.28 ±0.09	($\frac{3}{2}$ 1)	1 050	± 90	2.40 ±	0.30	2.39 ±0.50
461.00 ±0.50	$\frac{1}{2}$ 0	15 000	±1500			
466.20 ±0.50						1.57 ±0.40
468.82 ±0.09	$\frac{1}{2}$ 1	166	± 14			3.54 ±0.60[b]
470.00 ±0.09	$\frac{1}{2}$ 1	340	± 25			
474.18 ±0.09		143	± 12			
475.86 ±0.09		26	± 10			3.35 ±0.60[b]
486.98 ±0.10		70	± 9	1.41 ±	0.26	1.38 ±0.26

TABLE I. (*Continued*).

E_0 (keV)	J l	$g\Gamma_n$ (eV)	$\Delta g\Gamma_n$	$g\Gamma_Y$ (eV)	$\Delta g\Gamma_Y$	A (eV) ΔA
490.53 ±0.10	$\frac{3}{2}$ 1	376	± 30	1.09 ±	0.12	1.09 ±0.23
493.64 ±0.10	$\frac{1}{2}$ 0	196	± 25			
501.81 ±0.10	$\frac{3}{2}$ 1	193	± 16			
504.16 ±0.10	$\frac{3}{2}$ 1	283	± 23			
511.73 ±0.10	$\frac{1}{2}$ 1	149	± 12			
531.29 ±0.11	$\frac{1}{2}$ 1	477	± 52			
533.06 ±0.50	$\frac{1}{2}$ 0	5 300	± 530			
533.79 ±0.11	$\frac{3}{2}$ 1	541	± 54			
540.60 ±0.11	$\frac{3}{2}$ 1	846	± 68			
543.43 ±0.11	$\frac{1}{2}$ 1	134	± 17			
553.40 ±0.12	$\frac{3}{2}$ 1	706	± 70			
563.97 ±0.12	$\frac{3}{2}$ 1	402	± 32			
565.80 ±0.12		40	± 20			
569.89 ±0.12	$\frac{1}{2}$ 1	150	± 19			
573.33 ±0.13	$\frac{3}{2}$ 1	596	± 60			
577.56 ±0.13	$\frac{1}{2}$ 1	200	± 25			
580.30 ±0.13	$\frac{5}{2}$ 2	2400	± 190			
583.81 ±0.13		50	± 20			
585.19 ±0.13	$\frac{1}{2}$ 1	200	± 25			
591.84 ±0.13	$\frac{1}{2}$ 1	498	± 50			
599.02 ±0.14	$\frac{1}{2}$ 1	500	± 50			
604.63 ±0.14	$\frac{1}{2}$ 1	288	± 43			
608.19 ±0.14	$\frac{3}{2}$ 1	1284	± 103			
612.00 ±0.70	$\frac{1}{2}$ 0	16 000	±2000			
613.75 ±0.14	$\frac{3}{2}$ 2	1100	± 110			
618.81 ±0.14		48	± 16			
622.45 ±0.14	$\frac{1}{2}$ 1	525	± 53			
629.75 ±0.14	$\frac{3}{2}$ 1	840	± 85			
635.48 ±0.14	$\frac{3}{2}$ 1	1254	± 100			
638.36 ±0.14		112	± 37			
640.18 ±0.15	$\frac{3}{2}$ 1	772	± 77			
641.71 ±0.15	$\frac{1}{2}$ 1	305	± 33			
644.28 ±0.15		92	± 14			
651.68 ±0.15		76	± 15			
655.27 ±0.15	$\frac{1}{2}$ 1	280	± 28			
660.90 ±0.15		15	± 10			
668.25 ±0.15		55	± 11			
673.51 ±0.15	$\frac{1}{2}$ 1	175	± 16			
674.57 ±0.15	$\frac{1}{2}$ 1	626	± 50			
679.07 ±0.16		51	± 12			
685.23 ±0.16	$\frac{3}{2}$ 1	456	± 37			
687.46 ±0.16		118	± 12			
693.00 ±0.16	$\frac{1}{2}$ 1	252	± 25			
699.12 ±0.16		48	± 10			
706.02 ±0.17	$\frac{5}{2}$ 2	3600	± 290			
713.79 ±0.17	$\frac{1}{2}$ 1	4300	± 520			
715.81 ±0.17		200	± 40			

TABLE I. (*Continued*).

E_0 (keV)	J l	$g\Gamma_n$ (eV)	$\Delta g\Gamma_n$	$g\Gamma_Y$ (eV) $\Delta g\Gamma_Y$	A (eV) ΔA
720.30 ±0.17		200	± 50		
721.70 ±0.17		50	± 25		
725.30 ±0.17		200	± 50		
731.86 ±0.18	$\frac{1}{2}$ 1	700	± 140		
735.17 ±0.18		100	± 50		
737.03 ±0.18	$\frac{3}{2}$ 1	1000	± 100		
740.00 ±0.80	$\frac{1}{2}$ 0	30 000	±3500		
740.81 ±0.18	$\frac{3}{2}$ 1	740	± 75		
747.10 ±0.18	$\frac{5}{2}$ 2	4300	± 350		
757.81 ±0.19	$\frac{3}{2}$ 2	2200	± 180		
768.36 ±0.19	$\frac{3}{2}$ 1	1220	120		
771.89 ±0.50	$\frac{1}{2}$ 0	5820	± 600		
779.36 ±0.19	$\frac{1}{2}$ 1	600	± 60		
782.39 ±0.20		60	± 30		
787.33 ±0.20	$\frac{1}{2}$ 1	300	± 75		
793.30 ±0.90	$\frac{1}{2}$ 0	14 400	±1500		
801.83 ±0.20	$\frac{5}{2}$ 2	1350	± 110		
804.12 ±0.20	$\frac{1}{2}$ 1	800	± 160		
809.70 ±0.20	$\frac{1}{2}$ 1	700	± 140		
816.20 ±0.21	$\frac{1}{2}$ 1	1050	± 210		
821.70 ±0.21	$\frac{1}{2}$ 1	600	± 120		
841.20 ±0.42	$\frac{1}{2}$ 0	1520	± 170		
842.50 ±0.21		100	± 40		
850.10 ±0.21	$\frac{1}{2}$ 1	250	± 60		
863.60 ±0.22	$\frac{1}{2}$ 1	700	± 100		
866.00 ±0.22	$\frac{5}{2}$ 2	6600	± 900		
868.85 ±0.90	$\frac{1}{2}$ 0	6000	±1200		
869.60 ±0.22		500	± 150		
871.00 ±0.22	$\frac{1}{2}$ 1	2500	± 800		
872.00 ±0.22		200	± 60		
874.50 ±0.22		70	± 50		
878.80 ±0.23	$\frac{3}{2}$ 1	2000	± 300		
881.10 ±0.23	$\frac{1}{2}$ 1	700	± 140		
884.70 ±0.23	$\frac{1}{2}$ 1	350	± 70		
888.00 ±0.23	$\frac{1}{2}$ 0	1000	± 250		
888.80 ±0.23	$\frac{1}{2}$ 1	1000	± 150		
891.80 ±0.23	$\frac{1}{2}$ 1	400	± 80		
898.84 ±0.90	$\frac{1}{2}$ 1	7250	± 900		
899.80 ±0.24	$\frac{3}{2}$ 1	1600	± 240		
900.60 ±0.24		400	± 80		
910.70 ±0.24	$\frac{5}{2}$ 2	7500	±1125		
917.75 ±0.90	$\frac{1}{2}$ 0	5000	±1000		
935.00 ±0.25	$\frac{3}{2}$ 1	1000	± 150		
937.60 ±0.25	$\frac{1}{2}$ 1	400	± 135		
939.50 ±0.25	$\frac{5}{2}$ 2	3000	± 450		
940.60 ±0.25	$\frac{1}{2}$ 1	500	± 170		

TABLE I. (Continued).

E_0 (keV)	J l	$g\Gamma_n$ (eV)	$\Delta g\Gamma_n$	$g\Gamma_\gamma$ (eV)	$\Delta g\Gamma_\gamma$	A (eV)	ΔA
946.30 ±0.26		300	± 150				
952.60 ±1.00	$\frac{1}{2}$ 0	23 400	±4500				
953.20 ±0.26		150	± 75				
957.10 ±0.26	$\frac{3}{2}$ 1	2000	± 300				
960.30 ±0.26	$\frac{3}{2}$ 1	1400	± 700				
965.20 ±0.27		200	± 100				
969.90 ±0.27	$\frac{5}{2}$ 2	3300	± 600				
972.30 ±0.27		400	± 200				
982.30 ±0.27	$\frac{3}{2}$ 2	1200	± 200				
986.43 ±1.00	$\frac{1}{2}$ 0	2000	± 500				
993.50 ±0.28		300	± 150				
994.40 ±0.28		400	± 200				
1042.0	($\frac{1}{2}$ 0	25 000)					
1067.0	($\frac{1}{2}$ 0	6000)					

[a]Multiplet.
[b]A assigned to pair of resonances.

V. DISCUSSION OF RESULTS

The multilevel fit of the total neutron cross section is given in Figs. 1(a)–1(j) and part of the fitted neutron capture spectrum can be seen in Figs. 2(a)–2(e). The resulting resonance parameters are presented in Table I and will be compared with recent data of ORNL (Ref. 4) which was, until now, the most comprehensive data set available. Where discrepancies occur reference will be made to other literature.[2,21–24] It should be noted that the accelerator pulse widths of Geel and ORNL were comparable and that the latter measurements were 80 m time-of-flight transmission, as opposed to our 200 and 400 m. Our transmission data resolution is therefore comparatively better by up to a factor of 5 and we have, in addition, a neutron capture measurement at 60 m which is generally more sensitive to narrow resonances.

A. Resonance parameters

The analysis of the transmission data has been extended to 1 MeV and can be compared with ORNL results up to 910 keV wherein they assign 20 resonances as s waves, three of which we do not observe: namely, those at 251, 653, and 766 keV. Although we assign an additional three resonances in this energy range as s wave, giving a total of 20 up to 910 keV, the resulting plot of the level distribution shown in Fig. 3 is not as linear as might be expected. Two gaps are readily seen, from 140 to 265 keV and 612 to 750 keV. Figures 1(i) and 1(j) show that s-wave resonances, which would have an influence on these gaps, are not observed at 251 or 653 keV in our measurement. The three additional s-wave resonances at 493, 868, and 888 keV are a consequence of the improved resolution of the present measurement. While referring

to ORNL it should be noted that in Ref. 4 the distribution of s-wave resonances given in their Fig. 3 is not consistent with their Table II because resonances at 251 and 766 keV are not included in the plot. When comparing resonances with $l > 0$ with Ref. 4 we do not see any resonances in our data at 5.2, 183, 382, 536, 616, 683, 711, 757, 761, or 906 keV. Further comparison with other published data for all discrepant resonances shows Beer and Spencer[2] assigning the 251 keV level as s wave and Allen[23] assigning the 5.2, 183, and 251 keV levels with $l > 0$. All other discrepant levels are not noted.

From the neutron capture measurement data, the six lowest energy s waves were observable together with, up to 500 keV, 81 resonances having $l > 0$. Radiative capture parameters are presented alongside the transmission data in Table I for these resonances, of which only those at 57, 378, 470, and 474 keV were not satisfactorily resolved. The radiative widths of the large s-wave resonances, at 50, 96, and 140 keV, have been corrected for the neutron sensitivity of the capture detectors, the correction factors being 0.59, 0.75, and 0.45, respectively. Above 500 keV only transmission results are given due to the limitation of the capture data resolution at high energy. In total, 200 resonances have been analyzed up to 1 MeV of which 24 are s-wave and 12 are d-wave assigned, the majority (88) of the remainder being p-wave resonances. This is a substantial (25%) increase over the number of levels previously reported.

Detailed comparison with Ref. 4 shows our resonance energies of well-resolved sharp peaks to be systematically 0.1% higher. It should be noted that ORNL have since made a slight correction (+17 mm) to their flight-path length[25] which accounts for almost haf of this discrepancy and would bring the two energy data sets within the quoted errors. For s-wave levels our values of $g\Gamma_n$ are
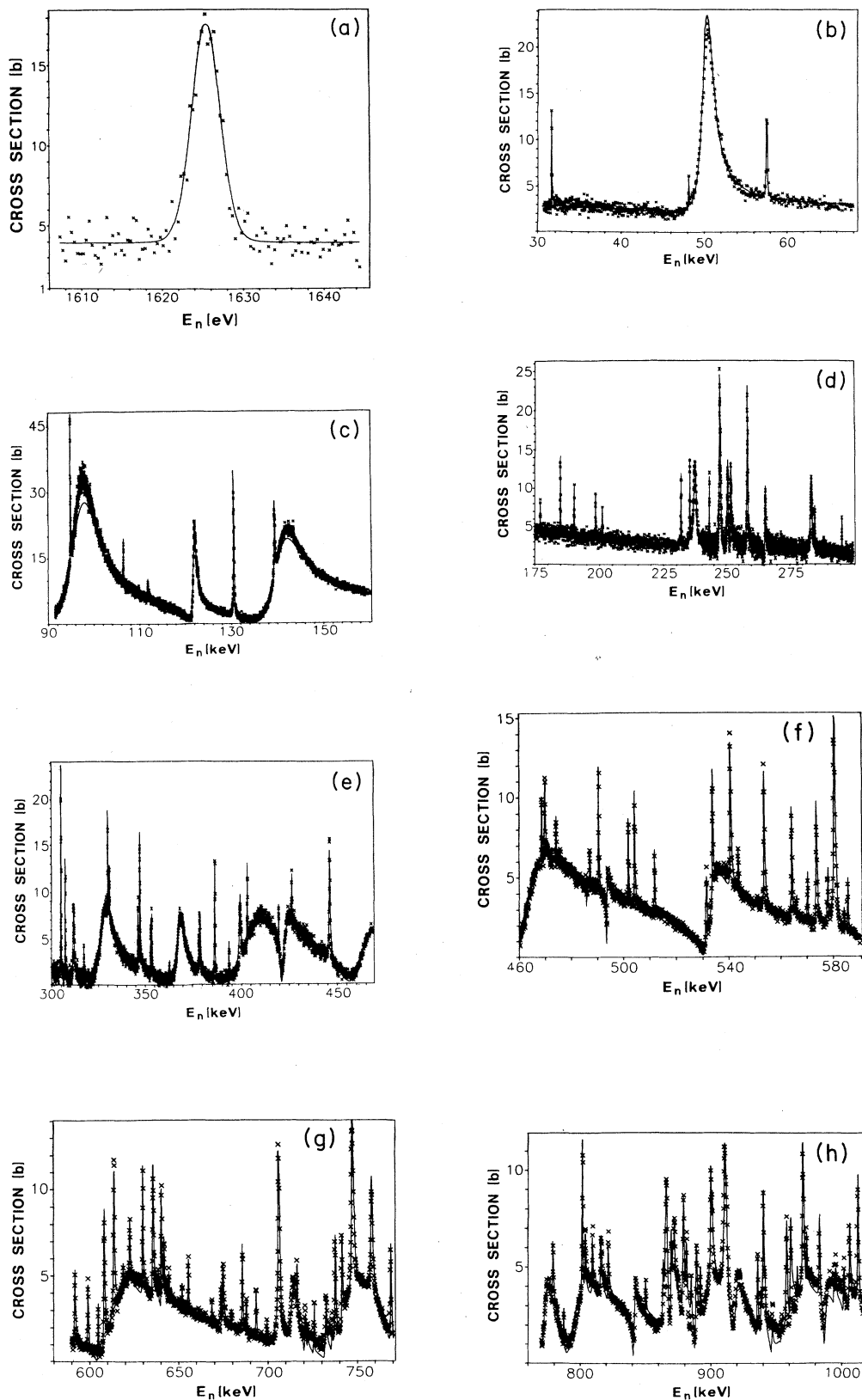
FIG. 1. Results from multilevel fits of the total neutron cross-section measurements. (i) and (j) give a more detailed view for reasons explained in the text.
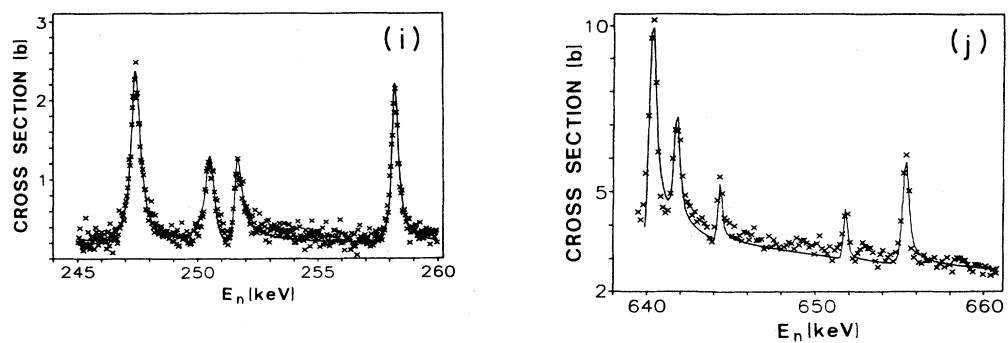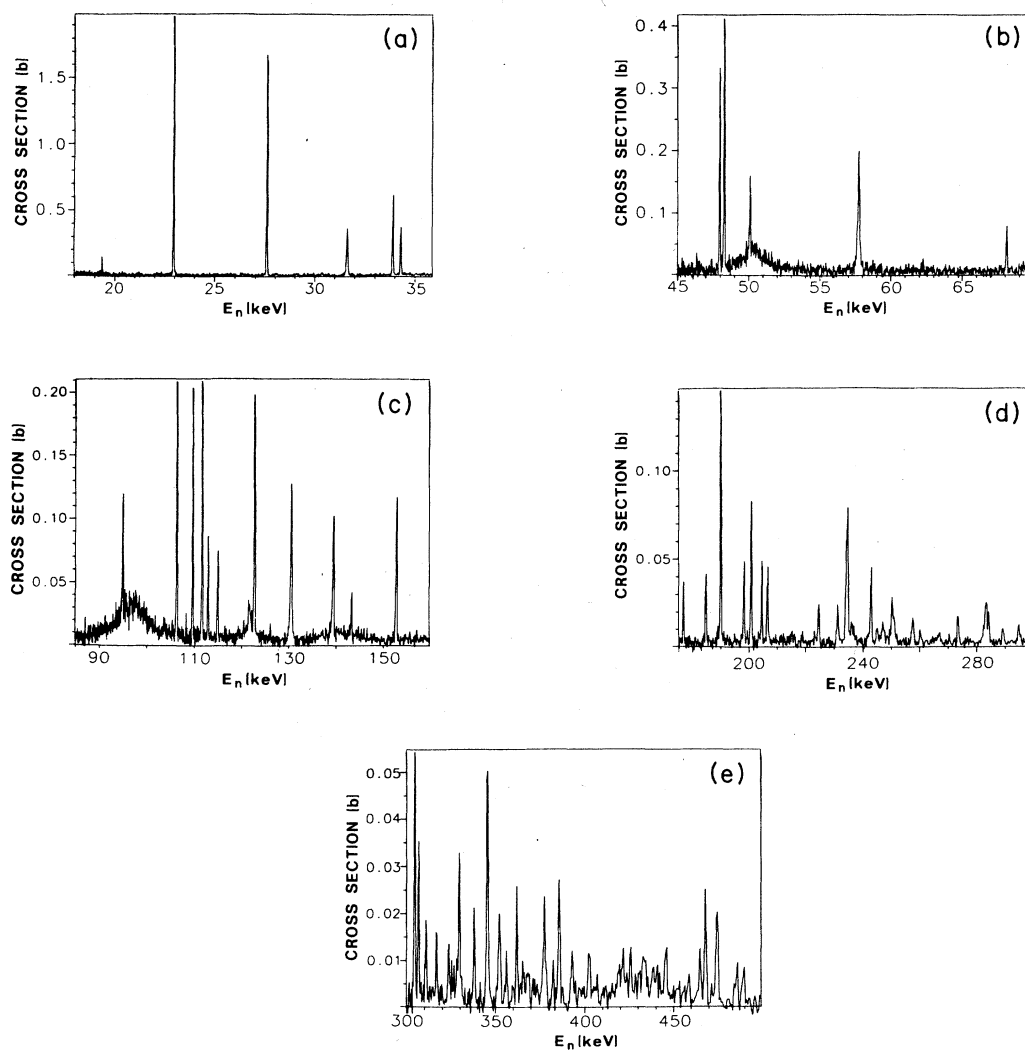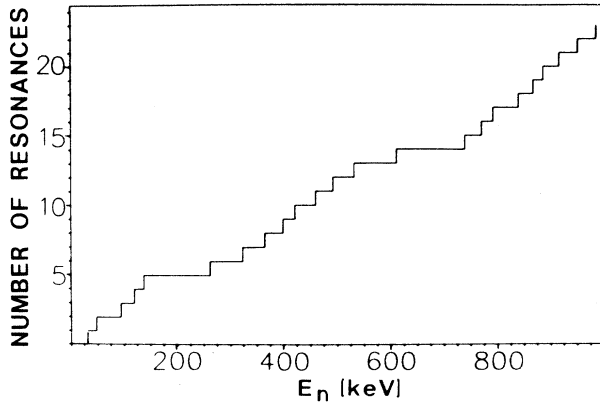
FIG. 1. (Continued).

FIG. 2. Neutron-capture cross section; doppler and resolution broadened and not corrected for multiple scattering nor prompt background.
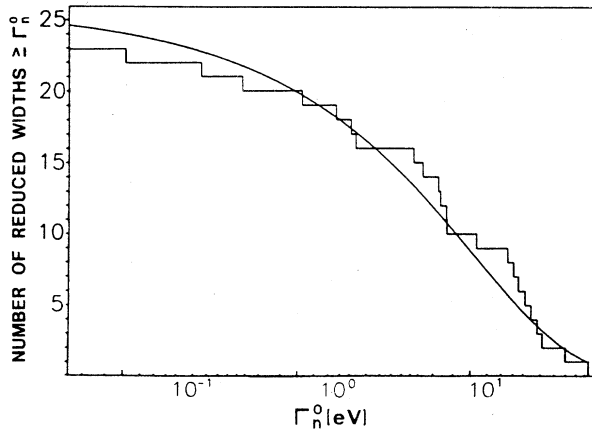
FIG. 3. Level distribution for resonances with $l = 0$.

TABLE II. The energy ranges, number of s-wave resonances and average level spacing of the three doorway structures for ^{52}Cr.

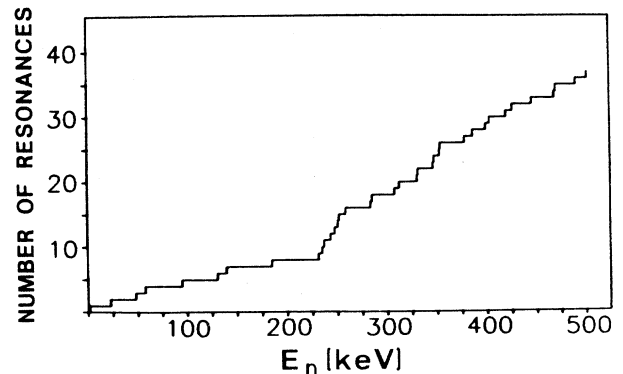| Energy range (keV)	Number of resonances	Average level spacing D_0 (keV)
31–140	5	27.1±6.3
265–612	9	43.4±7.5
740–986	9	30.8±5.3

generally larger up to 533 keV, above which the reverse is true. A similar comparison of $g\Gamma_n$ values for $l > 0$ resonances certainly shows considerable fluctuations although only in the energy range 450–600 keV are our values systematically larger. When comparing with Ref. 24 for ten well-resolved resonances ($l > 0$) up to an energy of 200 keV, our capture areas A are on average 4% lower.

B. Average level spacings and widths distribution

1. s waves

The s-wave level spacing has been determined for the 23 observed levels as $D_0 = (43.4 \pm 4.7)$ keV, in agreement with the ORNL value. In Fig. 3 the number of s-wave resonances is plotted against neutron energy and two interruptions are notable in the curve, each gap possibly representing three missing levels if a regular distribution is assumed. The gap at 200 keV is also observed in the ORNL data, whereas that at 650 keV is considerably reduced by their assignment of an s-wave resonance at 653 keV. In Fig. 4 the reduced neutron widths of the 23 s-

wave resonances are fitted with a theoretical Porter-Thomas distribution which indicates that only one, or maximum two, levels are missed. However, this is insufficient to explain the large gaps observed in the level distribution and has not been included in the level-spacing determination. The probability of having two such gaps has been estimated, by means of a Monte Carlo code based on a Wigner distribution, as 0.2% up to 1 MeV. The probability of a single gap is 2%.

The two gaps divide the resonances into three groups belonging to three separate doorway structures and, according to the level density systematics,[1] the fine-structure resonances are 3p-2h type. The separation of doorway structures becomes possible because the spread of the fine-structure resonances is smaller than the spacing of doorway states. The energy ranges and s-wave level spacings of the doorway structures are given in Table II. Similar small spreading of fine-structure states was observed in the alpha-cluster nuclei ^{32}S and ^{28}Si.[26]

2. p waves

Another even stronger discontinuity in the level spacing is observed for p-wave resonances as shown in Fig. 5. If the resonances up to 500 keV are considered, two regions can be distinguished where the level-spacing distribution is linear, namely the intervals (0–200) keV and (300–500) keV. The ranges are separated by a clustering of p-wave resonances at 250 keV. The strong increase in levels at about 250 keV can be interpreted as a threshold for additional resonances with higher hierarchy as discussed in Refs. 1 and 26. The level spacings in the inter-

FIG. 4. Histogram of reduced neutron widths for 23 s-wave resonances fitted with Porter-Thomas distribution over the energy range up to 1 MeV.

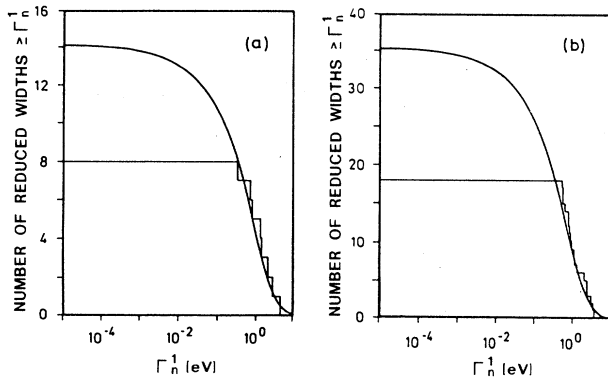FIG. 5. Level distribution for resonances with $l = 1$.

FIG. 6. Histograms of reduced neutron widths for p-wave resonances fitted with Porter-Thomas distributions; (a) energy range: (0–200) keV ($N = 14\pm4$); (b) energy range: (300–500) keV ($N = 35\pm5$).

vals (0–200) keV and (300–500) keV have been estimated by individual fitting with a Porter-Thomas distribution for the reduced widths, as shown in Fig. 6. This plot indicates 6 and 18 missed p-wave levels in the two energy regions, giving $D_1 = 14.7$ keV and $D_1 = 5.7$ keV, respectively, i.e., the level density parameter (a) exhibits a strong dependence upon the excitation energy. Such changes in a would be expected from the level density systematics discussed in Ref. 1, where a is a steplike function of atomic mass number.

C. Strength functions

1. s wave

The sum of the reduced neutron widths of s-wave resonances is plotted as a function of energy in Fig. 7. A linear fit of the data over the complete energy range gives the s-wave strength function $S_0 = (2.85\pm0.25)\times10^{-4}$. That we do not observe an energy dependence, as reported in Ref. 4, is explained by the discrepancies mentioned in Sec. V A, where we have compared the two data sets of neutron widths. The average values for S_0 in both sets
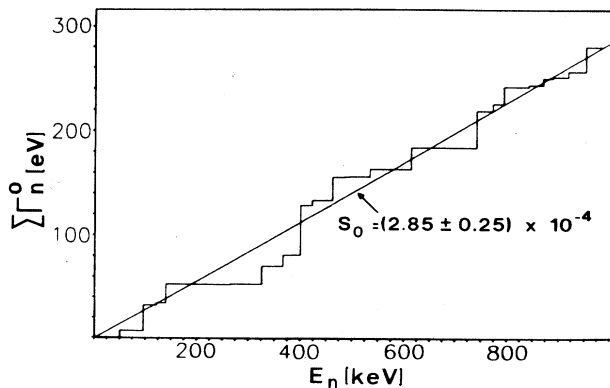
agree within 3%, but are 44% lower than predicted by the optical model.[27] As described in Ref. 4, where the authors compare the strength functions of two chromium isotopes with those calculated by Müller and Rohr,[3] the importance of the doorway concept for the strength function is demonstrated.

2. p wave

The p-wave strength function has been obtained from Fig. 8 as $S_1 = (0.30\pm0.05)\times10^{-4}$ in the energy range below 200 keV and agrees with the slope of the curve beyond 300 keV. The sudden step at 250 keV corresponds to a nonstatistical effect in the strength function at this energy and is also to be seen in the distribution of p-wave resonances. It is caused by the threshold effect of the fragmentation into more complicated states. Although there is a change in the level density below and beyond the threshold, of about a factor of 3, there is no change in the strength function value.

D. Parity dependence

The parity dependence of the level density of ^{52}Cr indicated in Ref. 4, i.e., the observation of 5.3 times more p-wave than s-wave levels, is based upon the assumption that apart from three d-wave resonances, all non-s-wave resonances are p wave. However we observe a considerable amount of d waves and also expect a portion of the unassigned small resonances to be so. Therefore our determination of the p-wave level density is based upon assigned p-wave resonances only, as described in Sec. V B 2. The results show a decrease in the level spacing with $D_1 = 14.7$ keV and $D_1 = 5.7$ keV in the energy ranges (0–200) keV and (300–500) keV, respectively. The level spacing of the low-energy interval is a factor of 3 smaller than the observed s-wave spacing and in agreement with the level statistics. However, in the higher-energy interval there are 7.8 times more p-wave resonances than s-wave resonances, indicating a local parity dependence. In the ORNL publication a parity dependence for the whole measured range has been stated.

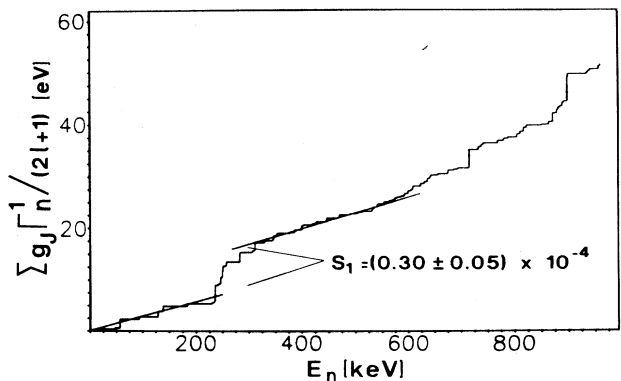The local parity dependence may be explained by hav-

FIG. 7. Sum of reduced neutron widths for 23 s-wave resonances plotted against energy.

FIG. 8. Sum of reduced neutron widths for p-wave resonances plotted against energy.

ing different energy thresholds, for s- and p-wave resonances, where the next hierarchy of states becomes energetically possible. According to the level density systematics[1] the s-wave resonances of ^{52}Cr, in the energy range covered by this paper, are 3p-2h states. In the energy range below 200 keV the p-wave level spacing is a factor of 3 smaller than the s-wave level spacing, in agreement with theory, indicating these p-wave resonances to be 3p-2h states. At approximately 250 keV, 4p-3h states become energetically possible for p-wave resonances and the corresponding level density increases considerably. This interpretation is in agreement with the p-wave strength function which is constant except at this threshold energy, as mentioned in Sec. V C 2.

VI. CONCLUSIONS

The measurements of ^{52}Cr and the analyses of resonance data for transmission up to 1 MeV and for capture up to 500 keV have produced a more complete resonance structure for this isotope. Compared to the recently published ORNL data our transmission data resolution is comparatively improved by up to a factor of 5, mainly because of the longer flight path which we have used. This has consequences for the analysis of resonance data. For instance, in the energy range up to 910 keV, ORNL assign 20 resonances as s wave, three of which we do not observe. The average level spacing is barely changed since we assign an additional three resonances in this energy range as s-wave resonances. In total 200 resonances have been analyzed up to 1 MeV of which 23 are s-wave resonances and 12 are d-wave assigned, the bulk of the remainder being p-wave resonances. This is a substantial (25%) increase in the number of levels previously reported.

The two gaps observed in the s-wave level distribution indicate three doorway structures with equal level spacing. These local level spacings are on average 22% lower than $D_0 = (43.4 \pm 4.7)$ keV obtained for the whole energy range. However, no energy dependence is observed for the s-wave strength function, a possible explanation for which would require data from several nuclei and is beyond the scope of this paper.[28]

Another even stronger discontinuity in the level spacing is observed for p-wave resonances. In the p-wave level distribution three energy ranges with a different level spacing may be distinguished. The level spacing decreases by a factor of 2.6 between the ranges (0–200) keV and (300–500) keV. In the transition region (200–300) keV an even smaller level spacing is observed, indicating a threshold behavior for a fragmentation to a higher hierarchy of states. The pronounced threshold behavior may be created by a doorway structure of small spreading width. Similar effects have been observed in ^{28}Si and ^{32}S which, like ^{52}Cr, have a multiple of four nucleons in the target nucleus. This behavior of the p-wave level spacing causes a local parity dependence due to different energy thresholds for 4p-3h states for s- and p-wave resonances. A change in the level density at the p-wave threshold is observed and changes the level density parameter (a) as a function of excitation energy, as expected from the level density systematics. The value for the s-wave strength function is 44% smaller than that predicted by the optical model and is in agreement with the doorway concept.

The accumulation of nonstatistical effects in ^{28}Si, ^{32}S, and as now shown in this paper for ^{52}Cr, strongly suggests that further high-resolution measurements should be performed on medium-light 4n target nuclei over an energy range of a few MeV to study the nucleon-nucleon interactions in nuclei.

ACKNOWLEDGMENTS

[1]G. Rohr, Z. Phys. A **318**, 299 (1984).

[2]H. Beer and R. R. Spencer, Nucl. Phys. **A240**, 29 (1975).

[3]K. N. Müller and G. Rohr, Nucl. Phys. **A164**, 97 (1971).

[4]H. M. Agrawal, J. B. Garg, and J. A. Harvey, Phys. Rev. C **30**, 1880 (1984).

[5]A. Brusegan et al., Proceedings of the International Conference on Nuclear Data for Basic and Applied Science, Santa Fe, 1985, edited by P. G. Young et al. (Gordon and Breach, New York, 1986), Vol. 2, p. 633.

[6]A. Bignami, C. Coceva, and R. Simonini, Euratom Report EUR 5157e, 1974.

[7]R. L. Macklin and J. H. Gibbon, Phys. Rev. **159**, 1007 (1967).

[8]G. Rohr, Proceedings of the Specialists Meeting on Fast Neutron Capture Cross Sections, Argonne, 1982, Argonne National Laboratory Report ANL-84-4.

[9]F. Corvi et al., Proceedings of Consultants Meeting on Nuclear Data for Structural Materials, Vienna, Austria, 1983, International Nuclear Data Committee Report INDC(NDS)-152L, 1984.

[10]F. G. Perey, Proceeding of the International Conference on Nuclear Data for Basic and Applied Science, Santa Fe, 1985, edited by P. G. Young et al. (Gordon and Breach, New York, 1986), Vol. 2, p. 1523.

[11]G. De Saussure, D. K. Olsen, and R. B. Perez, Oak Ridge National Laboratory Report ORNL/TM-6286, 1978.

[12]M. R. Bhat, Brookhaven National Laboratory Report BNL 50296, 1971.

[13]F. Gregson, M. F. James, and D. S. Norton, United Kingdom Atomic Energy Authority Report AAEW-M517, 1965.

[14]F. H. Fröhner, Kernforschungszentrum Karlsruhe Report KFK-2129, 1976.

[15]A. Brusegan et al., Proceedings of the International Conference on Neutron Physics and Nuclear Data, Harwell, 1978, Organization for Economic Co-operation and Development Report OECD/NEA, 1978.

[16]A. G. R. Stewart, Rev. Sci. Instrum. **54**, 1 (1983).

[17]F. G. Auchampaugh, Los Alamos Scientific Laboratory Report CA-5473-MS, 1974.

[18]C. Bastian, Angela Users' Guide, CBNM Geel (unpublished).

[19]F. H. Fröhner, General Atomic Report 6906, 1966.

[20]F. H. Fröhner, Kernforschungszentrum Karlsruhe Report KFK-2145, 1976.

[21]R. G. Stieglitz, R. W. Hockenbury, and R. C. Block, Nucl. Phys. **A163**, 52 (1971).

[22]C. D. Bowman, E. G. Bilpuch, and H. W. Newson, Ann. Phys. (N.Y.) **17**, 319 (1962).

[23]B. J. Allen, J. W. Boldeman, and R. L. Macklin, Nucl. Sci. Eng. **82**, 230 (1982).

[24]B. J. Allen and A. R. de L. Musgrove, Proceedings of the Conference on Neutron Data for Structural Materials for Fast Reactors, Geel, Belgium, 1977 (unpublished); see also Australian Atomic Energy Commission Report E-400, 1977.

[25]D. C. Larson *et al.*, Oak Ridge National Laboratory Report ORNL/TM-9097, 1985.

[26]G. Rohr, *Proceedings of the 6th International Conference on Capture Gamma-Ray Spectroscopy, Leuven, Belgium, 1987,* edited by K. Abrahams and P. Van Assche (Insitute of Physics, Bristol, 1988), p. 643.

[27]B. Buck and F. Perey, Phys. Rev. Lett. **8**, 444 (1962).

[28]G. Rohr, International Conference on Nuclear Data for Science and Technology, Mito, Japan, 1988.